Computational Materials Science 183 (2020) 109753

Contents lists available at ScienceDirect

Computational Materials Science

journal homepage: www.elsevier.com/locate/commatsci

Effects and correction of angular momentum non-conservation in RNEMD for calculating thermal conductivity

Hong-Ao Yang (杨鸿澳), Bing-Yang Cao (曹炳阳)*

Key Laboratory for Thermal Science and Power Engineering of Ministry of Education, Department of Engineering Mechanics, Tsinghua University, Beijing 100084, China

ARTICLE INFO

Keywords:
Thermal conductivity
Reverse non-equilibrium molecular dynamics
Angular momentum
High heat flux

ABSTRACT

The effects of angular momentum non-conservation in reverse non-equilibrium molecular dynamics (RNEMD) for thermal conductivity calculation are investigated. The velocity swapping operation in RNEMD results in an abnormal angular momentum flux when the center-of-mass velocity of heat source is considerable. The angular momentum is found to motivate a nonphysical wave motion at high heat flux, which was regarded as a novel heat conduction mechanism in earlier researches. This additional heat transport channel may lead to a nonphysical increase in the computed thermal conductivity. Therefore, we propose an improved RNEMD, in which the hottest/coldest atoms are selected in center-of-mass frames. The results show that the improved RNEMD can greatly reduce the nonphysical correlation at any heat flux, eliminate the wave motion mode, and give constant thermal conductivity. Our research reveals a nonphysical effect from angular momentum non-conservation in RNEMD, and provides an improved RNEMD for heat transport in solid materials.

1. Introduction

Molecular dynamics (MD) simulation is a powerful way to study nanoscale heat transport. Based on Newton's law of motion and interatomic potentials, it traces trajectories of all atoms, providing a direct approach to study nanoscale heat conduction mechanisms. Molecular dynamics has been successfully applied to study thermal conductivities [1–4], phonon mean free path [5], phonon modes [6,7] and heat transport across interfaces [8–10]. There are two typical methods to simulate thermal properties, i.e., Equilibrium Molecular Dynamics (EMD) and Non-Equilibrium Molecular Dynamics (NEMD). In EMD, the Green-Kubo method is commonly used to compute thermal conductivity from the heat current autocorrelation function. It is based on the linear response theorem [11], hence valid in the linear regime but invalid in the nonlinear regime [12]. In addition, long simulation time is needed to get converged heat current autocorrelation function [13,14]. In NEMD, the thermal conductivity is computed directly from Fourier's law

$$J_\mu = -\sum_\nu k_{\mu\nu}\frac{\partial T}{\partial x_\nu}. \tag{1}$$

This method requires a steady temperature gradient and heat current. One way is to establish the temperature gradient by keeping the heat source and heat sink at different temperatures by thermostats, like Berendsen [15], Nosé-Hoover [16,17] and Langevin [18,19] thermostats. Another typical way is Reverse Non-Equilibrium Molecular Dynamics (RNEMD) proposed by Müller-Plathe in 1997 [14], which introduces a heat flux between heat sink and heat source to motivate temperature gradient. It reverses the cause-and-effect relationship between heat flux and temperature gradient. The RNEMD method has been successfully used in various kinds of materials, such as silicon [20], grapheme [3,21] and carbon nanotubes [1,22], and was proved effective. Since the heat flux can be directly extracted from the algorithm, it greatly reduces the computation costs. Its convergence time is similar with other NEMD methods, much shorter than EMD.

The RNEMD method works as follows. For every several time steps, select N hottest atoms in heat sink and N coldest atoms in heat source, then swap their velocities. Since the velocity distributions in the slabs are wide enough, the hottest atoms in heat sink are expected to be hotter than the coldest atoms in heat source. This operation introduces a heat flux between the heat sink and the heat source, and finally reaches a stable state. By changing the frequency of swap operation and the number of atoms to be swapped, the heat flux applied to the system can be regulated. The heat flux in each swap operation is given by:

$$J = \frac{\sum_i^{N_{swap}} \frac{m}{2}(v_{ih}^2 - v_{ic}^2)}{2t\cdot L_y L_z}, \tag{2}$$

where N_{swap} is the number of atoms swapped, m is the mass of atom, v_{ih}

* Corresponding author.
E-mail address: caoby@tsinghua.edu.cn (B.-Y. Cao).

https://doi.org/10.1016/j.commatsci.2020.109753
Received 3 March 2020; Received in revised form 14 April 2020; Accepted 15 April 2020

is the velocity of ith hottest atom in heat sink, v_{ic} is the velocity of ith coldest atom in heat source. t is the time interval between each swap operation. L_y and L_z are the size of system along y direction and $z$direction, respectively, assuming that the heat flux is along x direction.

It is obvious that the total energy and momentum of the system are conserved in this algorithm, but the angular momentum is not conserved. Müller-Plathe guessed that this "should normally not be a problem" [14]. This is true since the angular momentum flux seems to be completely random in most cases. But no researches have investigated when the angular momentum flux will go nonrandom and its consequence. The influence of the angular momentum non-conversation in the simulations of heat conduction remains unclear.

Recently, using RNEMD, several researches reported a wave motion heat conduction mechanism at high heat flux in materials like carbon nanotubes [23], graphene [24], graphene nanoribbons [25] and hybrid graphene/silicene monolayers [26]. The wave motion transport mode is triggered at high heat flux and forms a wave-like temperature profile. It provides an additional channel of heat conduction and thus greatly increases thermal conductivity of these materials at high heat flux. In the view of phonons, a specific low frequency acoustic phonon mode is enhanced and goes ballistic, resulting in non-Fourier transport of heat. But unfortunately, this heat conduction mechanism was never demonstrated experimentally.

In this paper, we reveal that the wave motion heat conduction mode is just the consequence of the angular momentum non-conservation in RNEMD. The angular momentum introduced by RNEMD is found to regularly fluctuate at the frequency of the wave motion. By analyzing the Pearson correlation coefficient (r) between the angular momentum flux and the center-of-mass (COM) velocity of slabs, a strong linear correlation ($r > 0.9$) between these two factors at high heat flux confirms that the angular momentum flux introduced by RNEMD is the source of the wave motion heat conduction. Further, we present a correction to the original RNEMD method to eliminate the regular angular momentum flux and keep the angular momentum flux random at any heat flux.

2. Method

All the MD simulations in this paper are performed using the LAMMPS package [27]. Graphene is taken as a case study (silicon cases in Supplementary material). The computational system contains 160 × 20 unit cells with 6400 carbon atoms as shown in Fig. 1. Periodic boundary conditions are employed in the in-plane directions. The time step in the whole simulation is set to 0.5 fs. The Tersoff potential [28] is used to describe the C–C interactions. It is a widely used many-body potential model for silicon, carbon and germanium, which can be expressed by

$$
\begin{aligned}
V_{ij} &= f_{ij}^{C}\left(Ae^{-\lambda_1 r_{ij}} - b_{ij}Be^{-\lambda_2 r_{ij}}\right) && \text{(3a)}\\
f_{ij}^{C} &= \begin{cases} 1, & r_{ij} < R - D; \\ \frac{1}{2} - \frac{1}{2}\sin\left(\frac{\pi}{2}\frac{(r_{ij}-R)}{D}\right), & R - D < r_{ij} < R + D; \\ 0, & r_{ij} > R + D; \end{cases} && \text{(3b)}\\
b_{ij} &= (1 + \beta^n \zeta_{ij}^n)^{-\frac{1}{2n}} && \text{(3c)}\\
\zeta_{ij} &= \sum_{k\neq i,j} f_{ik}^{C} g(\theta_{ijk}) e^{\lambda_3^m (r_{ij}-r_{ik})^m} && \text{(3d)}\\
g(\theta_{ijk}) &= \gamma_{ijk}\left(1 + \frac{c^2}{d^2} - \frac{c^2}{d^2 + (\cos\theta - \cos\theta_0)^2}\right) && \text{(3e)},
\end{aligned}
\tag{3}
$$

where f_{ij}^{C} is a cutoff function, $Ae^{-\lambda_1 r_{ij}}$ and $Be^{-\lambda_2 r_{ij}}$ are repulsive and attractive parts of the Morse potential, respectively. b_{ij} denotes the many-body effects depending on bond angles θ_{ijk}. Potential parameters modified for graphene are taken from Lindsay's research [29].

According to the RNEMD method, the system is divided into 40 slabs in the x direction. The 1st slab is appointed as heat sink and the 21st slab as heat source. First of all, the system is relaxed at 300 K by the NVT ensemble for 1 ns. Then, run RNEMD for 3 ns to reach a stable state and another 2 ns to collect time-averaged data. To apply different heat fluxes, the interval between each velocity swapping operation ranges from 10 time steps to 200 time steps and the number of swapped atoms ranges from 1 to 3. We also change the system length since it has significant influence on the thermal conductivity of grapheme [30]. Then, keeping all other settings the same, we run our improved RNEMD as a contrast. Details of the improved RNEMD will be discussed later. For each simulation, we extract the temperature and center-of-mass velocity (v_{COM}) of the 40 slabs every 10 time steps. In addition, the momentum exchange (momentum exchange is proportional to angular momentum flux), v_{COM} of heat sink and v_{COM} of heat source are also output in each velocity swapping operation.

3. Results of original RNEMD

Typical temperature profiles at a high heat flux of 1580 GW m^{-2} are presented in Fig. 2. The wave-like temperature profile is consistent with that in earlier researches [24]. As described in literature [23–25], the kinetic temperature, center-of-mass (COM) temperature, real temperature and center-of-mass velocity are defined as

$$
\begin{aligned}
T_{kinetic} &= \frac{2}{3k_B N}\sum_{i=1}^{N}\frac{1}{2}mv_i^2 && \text{(4a)}\\
T_{COM} &= \frac{2}{3k_B}\times\frac{1}{2}mv_{COM}^2, \quad \left(v_{COM} = \frac{1}{N}\sum_{i=1}^{N} v_i\right) && \text{(4b)}\\
T_{real} &= \frac{2}{3k_B N}\sum_{i=1}^{N}\frac{1}{2}m(v_i - v_{COM})^2 && \text{(4c)},
\end{aligned}
\tag{4}
$$

in which k_B is the Boltzmann constant, N is the number of atoms in a slab and v_i is the velocity of atom i. $T_{kinetic}$ represents the total kinetic energy, T_{COM} the center-of-mass kinetic energy, and T_{real} the real internal kinetic energy. The three definitions of temperature satisfy $T_{kinetic} = T_{COM} + T_{real}$. At such a high heat flux, two separated channels of heat conduction were thought to play a significant role. One is just the traditional Fourier's heat transport, presented by the real temperature profile. The other is the wave motion heat transport triggered at high heat fluxes, presented by the COM temperature profile. As shown in Fig. 2, the wave-like distribution of kinetic temperature comes from the

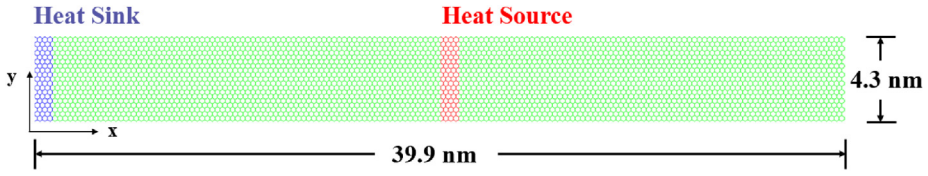

Fig. 1. Schematic of the simulation system.

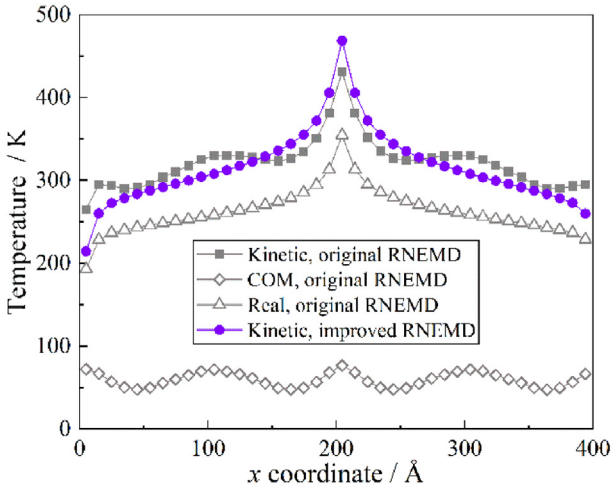

Fig. 2. Profiles of kinetic temperature, COM temperature and real temperature of original RNEMD at 1580 GW m^{-2}, and profile of kinetic temperature of improved RNEMD at 1369 GW m^{-2}.

center-of-mass kinetic energy, while the real temperature profile is similar with that at low heat flux. Earlier investigations have demonstrated that the Fourier's heat transport part results in the same thermal conductivity as low heat fluxes, while the wave transport provides an additional channel of heat transport [23,24]. The percentage of wave-transported energy could exceed 90% at high heat fluxes. We calculate the mode temperature of ballistic low frequency ZA phonon (i.e. mechanical wave) using spectral phonon temperature (SPT) method [6], and find it can be higher than 4×10^4 K.

We then examine the accumulated momentum exchange in RNEMD (momentum exchange is proportional to angular momentum flux). Fig. 3a shows the accumulated momentum exchange in a time period of 100 picoseconds, which has an obvious periodicity. The periodic momentum exchange means a nonphysical regular angular momentum flux is input into the system. Fig. 3b shows the Fourier transformation of the accumulated momentum exchange. As expected, the frequency of the accumulated momentum exchange fluctuation and that of the wave motion are the same. From the movie (see Supplementary Movie 1), it can be seen that the heat source acts like a mechanical "wave source" driven by a periodic force while the heat sink acts like a "wave sink". The wave motion is not spontaneous but driven by a periodic force. The driven force actually comes from the angular momentum flux in the RNEMD because it is the only possible external excitation in the simulations.

We evaluate the correlation of the momentum exchange and the center-of-mass velocity (v_{COM}) of the heat sink in each swap. A sample of 2000 pairs of data is plotted in Fig. 4a. These two quantities have a nearly linear correlation, which can be evaluated by the Pearson correlation coefficient (r). The Pearson correlation coefficient between A and B is given by

$$r(A, B) = \frac{1}{N-1} \sum_{i=1}^{N} \left(\frac{A_i - \mu_A}{\sigma_A} \times \frac{B_i - \mu_B}{\sigma_B} \right), \quad (5)$$

where μ_A and μ_B are the average value of A and B, respectively. σ_A and σ_B are the standard deviation of A and B, respectively. The sample data in Fig. 4a has a high Pearson correlation coefficient $r = 0.902$, which means a strong linear correlation. Although our data does not obey joint normal distribution, the Pearson correlation coefficient can still help us to compare the degree of correlation in different cases.

Further, we investigate the Pearson correlation coefficient at various heat fluxes and system lengths as shown in Fig. 5a. The lowest heat flux reaches 94 GW m^{-2}, which is low enough to be used in the calculation of heat transfer coefficient [30]. The significant increase of r corresponds to the formation of mechanical wave. The critical heat flux to trigger the wave-like heat transport mode is about 700 GW m^{-2}, independent of the system length. At high heat fluxes, the Pearson correlation coefficient is up to 0.9. It is worth noting that $r > 0.15$ even at low heat fluxes, which means there is still a very weak correlation. This will normally not influence the heat transfer coefficient calculation, but may have effects on phonon modes.

The computed thermal conductivity at different heat fluxes and system lengths is shown in Fig. 5b. We can see that k increases significantly at high heat fluxes because the excited wave motion provides an additional heat conduction channel. The critical heat flux when k increases non-physically is about 700 GW m^{-2}, independent of system length. The corresponding r is around 0.5, indicating that a medium linear correlation will lead to errors in thermal conductivity computation.

We turn our attention to the dependence of momentum exchange on v_{COM} of heat sink. In the RNEMD method, the center-of-mass velocities of slabs were not concerned while selecting the hottest atoms in heat sink and the coldest atoms in heat source. When v_{COM} is close to zero, the angular momentum flux is nearly white noise and has no significant influence on the computed thermal conductivity. When v_{COM} is nonzero, the atom velocities will follow a nearly isotropic distribution superimposing the center-of-mass velocity. The highest velocity is in the same direction of v_{COM}, and the lowest velocity is close to zero if the distribution is wide enough. So, the selected "hottest" atom in heat sink moves in the same direction of heat sink, while the velocity of the coldest atom in heat source is nearly isotropic but close to zero. As a consequence, the momentum exchange depends on the center-of-mass velocity of heat sink. The higher the center-of-mass velocity, the stronger the dependency. In solid materials, the regular angular momentum flux enhances specific low frequency acoustic phonon modes

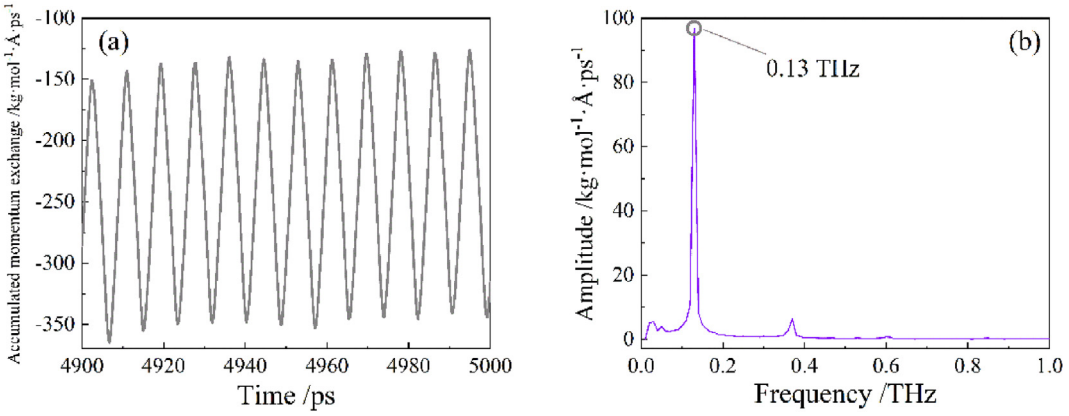

Fig. 3. Accumulated momentum exchange as a function of time (a) and its Fourier transformation (b).

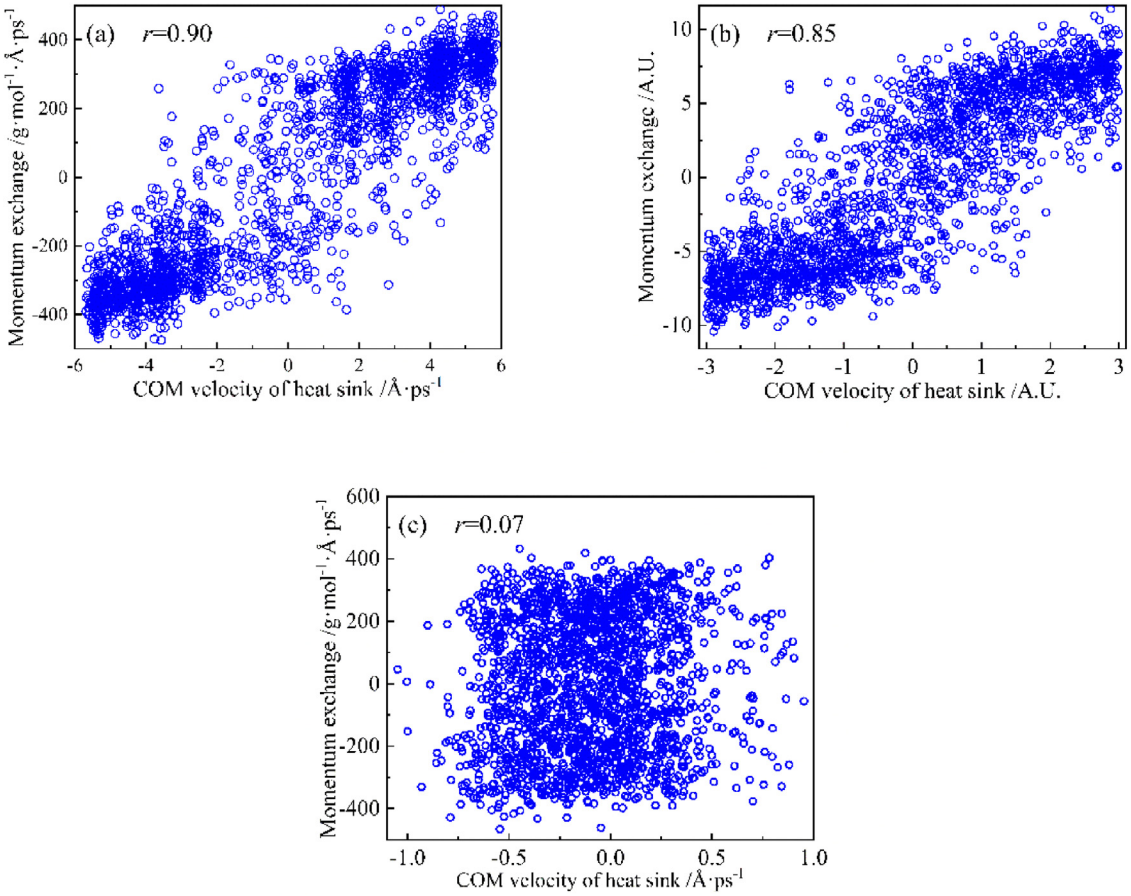

Fig. 4. Distribution of momentum exchange and v_{COM} of the heat sink and their Pearson correlation coefficient in (a) original RNEMD, (b) numerical simulations on original RNEMD and (c) improved RNEMD.

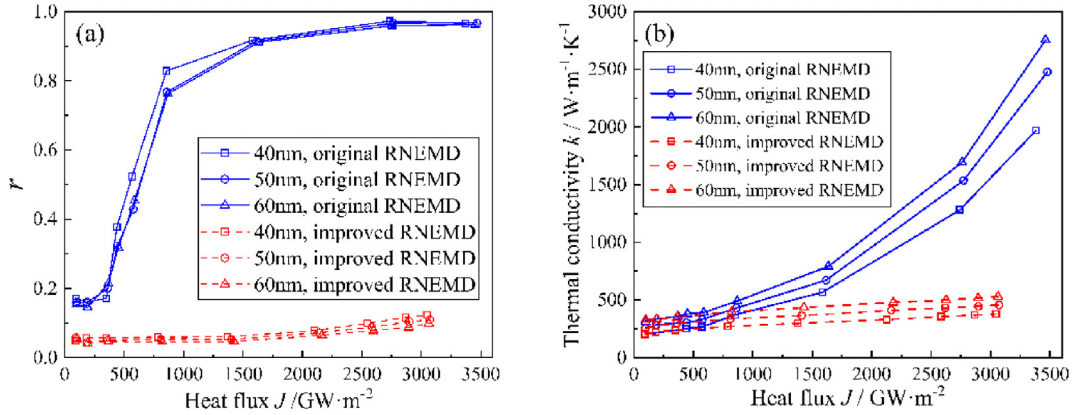

Fig. 5. (a) Pearson correlation coefficient and (b) Thermal conductivity as a function of heat flux in systems of different lengths using original RNEMD and improved RNEMD.

and forms a positive feedback. When the heat flux is high enough, the system finally falls into a mechanical wave motion mode.

To test our hypothesis, numerical simulations are performed. Assuming that the velocities of atoms in each slab consist of a Maxwell velocity distribution and an additional overall velocity, 2000 swaps are performed, and the results are shown in Fig. 4b. The joint distribution exhibits strong linearity and concentrates in the first and third quadrants, which is similar to that in Fig. 4a, confirming our hypothesis. It is also demonstrated that the coldest atoms in heat source have close-to-zero velocities, and it will not influence the momentum exchange.

4. Improved RNEMD

To eliminate the bias in atom selection, we here suggest an improved RNEMD method. That is, select the hottest and coldest atoms in the center-of-mass (COM) frames of heat sink and heat source. The original RNEMD selects the hottest and coldest atoms by kinetic temperature, while our improved RNEMD selects by real temperature. The heat flux in each swap in the improved RNEMD is given by

$$J = \frac{\sum_{i}^{N_{swap}} \frac{m_i}{2}(v_{ih,COM}^2 - v_{ic,COM}^2)}{2t \cdot L_y L_z}, \quad (6)$$

where $v_{ih,COM}$ is the velocity of the ith hottest atom in the heat sink COM frame and $v_{ic,COM}$ is the velocity of the ith coldest atom in the heat source COM frame. All other parameters are the same with those in the original RNEMD. The correction is reasonable in physics since the concept of "hot" and "cold" is supposed to be defined in the COM frames. Meanwhile, the correction retains most properties of the original RNEMD method because it only optimizes the atom selection strategy.

The temperature profile of the improved RNEMD at a heat flux of 1369 GW m^{-2} is shown in Fig. 2, which shows good linearity, in good agreement with the temperature profile at low heat fluxes. The wave-like temperature profile disappears, so does the wave motion (see Supplementary Movie 2). Actually, the COM temperature in the improved RNEMD is lower than 2.5 K, which can be ignored. We also examine the amount of momentum exchange in the improved RNEMD and v_{COM} of the heat sink in each swap operation. A set of 2000 pairs data in the last 20 picoseconds of the simulation is plotted in Fig. 4c. It can be seen that they distribute more evenly that those in Fig. 4a. The Pearson correlation coefficient of these 2000 pairs data is only 0.0791, indicating no linear correlation.

Then we study the dependency of Pearson correlation coefficient on heat flux and system length. The results are shown in Fig. 5a by dashed lines. It is clear that the improved RNEMD has a lower r that the original RNEMD at any heat flux. r was controlled below 0.1 in the improved RNEMD at high heat fluxes, which means the dependence is extremely weak to be ignored. The mechanical wave could not be triggered at high heat flux in improved RNEMD.

The thermal conductivity k at different heat fluxes and system lengths is presented in Fig. 5b. At low heat fluxes, the results of the improved RNEMD and the original RNEMD match excellently. At high heat fluxes, however, k is influenced by the wave motion heat conduction in the original RNEMD, but holds nearly constant in the improved RNEMD. So, it is necessary to check whether the nonphysical wave motion is triggered in the original RNEMD, but the improved RNEMD avoids the problem at any heat fluxes. In addition, at any heat fluxes, the original RNEMD may influence the transport of phonons because it introduces an extra angular momentum flux to the system, while the improved RNEMD eliminates it.

Further, we have tested the original and improved RNEMD on silicon at various heat fluxes and compared with the results of NEMD using Nose-Hoover and Langevin thermostats (see Supplementary material). Wave motion in silicon is triggered in the original RNEMD at high heat fluxes and can be eliminated in the improved RNEMD, just like those in graphene. The computed thermal conductivity using the improved RNEMD is consistent with that using Nose-Hoover thermostat. The improved RNEMD can be extended to most solid materials and eliminate the nonphysical angular momentum flux.

5. Conclusions

In this paper, we investigate the influence of angular momentum flux in RNEMD. At high heat fluxes, the angular momentum flux fluctuates regularly, resulting in an anomalous wave motion transport phenomenon. The regular fluctuation rises because the center-of-mass velocity is not concerned in hottest/coldest atom selection in the original RNEMD, and the angular momentum flux is related to the COM velocity of slabs. We evaluate the correlation using Pearson correlation coefficient, over 0.9 in the original RNEMD. Then we propose an improved RNEMD in which the hottest and coldest atoms are selected in COM frames. The improved RNEMD can decrease the Pearson correlation coefficient below 0.1, almost eliminating the correlation. The improved RNEMD has the following advantages.

1. *Inheritance*. The improved RNEMD inherits almost all the advantages of the original RNEMD.
2. *Physical rationality*. The improved RNEMD defines the hottest and coldest atoms by real temperature, which is more rational in physics.
3. *Random angular momentum flux*. The randomicity of angular momentum flux in the improved RNEMD is higher than the upper bound in the original RNEMD at any heat flux. The success of the improved RNEMD has demonstrated that such a random angular momentum flux is acceptable.
4. *Constant thermal conductivity*. The improved RNEMD gives the same thermal conductivity as the original RNEMD at low heat flux and keeps constant when heat flux goes high but the original RNEMD loses efficiency.

When using the original RNEMD to simulate nanoscale heat transport in solid materials, it is necessary to keep an eye on the angular momentum flux introduced by algorithm and keep alert when it loses randomness. However, the improved RNEMD ensures the randomness of angular momentum flux and works no worse than the original RNEMD at any heat fluxes, so it is more convenient and efficient.

Declaration of Competing Interest

The authors declare that they have no known competing financial interests or personal relationships that could have appeared to influence the work reported in this paper.

CRediT authorship contribution statement

Hong-Ao Yang: Conceptualization, Methodology, Software, Investigation, Validation, Formal analysis, Data curation, Visualization, Writing - original draft. **Bing-Yang Cao:** Methodology, Supervision, Project administration, Funding acquisition, Writing - review & editing.

Acknowledgments

The authors would like to thank Jin Wang and Ji-Hang Zou (Department of Engineering Mechanics, Tsinghua University) for useful discussion. This work is supported by the National Natural Science Foundation of China (Grant No. 51825601, 51676108).

Data availability

The raw data required to reproduce these findings are available to download from http://dx.doi.org/10.17632/433jx6h3mf.1. The processed data required to reproduce these findings are available to download from http://dx.doi.org/10.17632/433jx6h3mf.1.

Appendix A. Supplementary data

Supplementary data to this article can be found online at https://doi.org/10.1016/j.commatsci.2020.109753.

References

[1] H. Zhao, et al., Thermal conductivities of graphyne nanotubes from atomistic simulations, Comput. Mater. Sci. 106 (2015) 69–75, https://doi.org/10.1016/j.commatsci.2015.04.042.
[2] A. Tabarraei, Thermal conductivity of monolayer hexagonal boron nitride nanoribbons, Comput. Mater. Sci. 108 (2015) 66–71, https://doi.org/10.1016/j.commatsci.2015.06.006.
[3] Y.-Y. Zhang, Q.-X. Pei, C.-M. Wang, A molecular dynamics investigation on thermal conductivity of graphynes, Comput. Mater. Sci. 65 (2012) 406–410, https://doi.org/10.1016/j.commatsci.2012.07.044.
[4] J.-N. Hu, X.-L. Ruan, Y.-P. Chen, Thermal conductivity and thermal rectification in graphene nanoribbons: a molecular dynamics study, Nano Lett. 9 (2009) 2730–2735, https://doi.org/10.1021/nl901231s.

[5] B. Qiu, et al., Molecular dynamics simulations of lattice thermal conductivity and spectral phonon mean free path of pbte: bulk and nanostructures, Comput. Mater. Sci. 53 (2012) 278–285, https://doi.org/10.1016/j.commatsci.2011.08.016.
[6] T.-L. Feng, et al., Spectral analysis of nonequilibrium molecular dynamics: spectral phonon temperature and local nonequilibrium in thin films and across interfaces, Phys. Rev. B 95 (2017), https://doi.org/10.1103/PhysRevB.95.195202.
[7] J.-H. Zou, X.-T. Xu, B.-Y. Cao, Size-dependent mode contributions to the thermal transport of suspended and supported graphene, Appl. Phys. Lett. 115 (2019), https://doi.org/10.1063/1.5115060.
[8] K. Gordiz, A. Henry, Phonon transport at interfaces: determining the correct modes of vibration, J. Appl. Phys. 119 (2016) 015101, , https://doi.org/10.1063/1.4939207.
[9] J.-H. Zou, G.-J. Hu, G.-X. Cao, Enhanced thermal transport across multilayer graphene and water by interlayer functionalization, Appl. Phys. Lett. 112 (2018) 041603, , https://doi.org/10.1063/1.5018749.
[10] T.-L. Feng, et al., Unexpected high inelastic phonon transport across solid-solid interface: modal nonequilibrium molecular dynamics simulations and landauer analysis, Phys. Rev. B 99 (2019), https://doi.org/10.1103/PhysRevB.99.045301.
[11] R. Kubo, Statistical-mechanical theory of irreversible processes. 1. General theory and simple applications to magnetic and conduction problems, J. Phys. Soc. Jpn. 12 (1957).
[12] D.J. Searles, D.J. Evans, The fluctuation theorem and green-kubo relations, J. Chem. Phys. 112 (2000) 9727–9735, https://doi.org/10.1063/1.481610.
[13] M.H. Khadem, A.P. Wemhoff, Comparison of green-kubo and nemd heat flux formulations for thermal conductivity prediction using the tersoff potential, Comput. Mater. Sci. 69 (2013) 428–434, https://doi.org/10.1016/j.commatsci.2012.12.016.
[14] F. Müller-Plathe, A simple nonequilibrium molecular dynamics method for calculating the thermal conductivity, J. Chem. Phys. 106 (1997) 6082–6085, https://doi.org/10.1063/1.473271.
[15] H.J.C. Berendsen, et al., Molecular-dynamics with coupling to an external bath, J. Chem. Phys. 81 (1984) 3684–3690, https://doi.org/10.1063/1.448118.
[16] S. Nose, A unified formulation of the constant temperature molecular-dynamics methods, J. Chem. Phys. 81 (1984) 511–519, https://doi.org/10.1063/1.447334.
[17] W.G. Hoover, Canonical dynamics – equilibrium phase-space distributions, Phys. Rev. A 31 (1985) 1695–1697, https://doi.org/10.1103/PhysRevA.31.1695.
[18] T. Schneider, E. Stoll, Molecular-dynamics study of a 3-dimensional one-component model for distortive phase-transitions, Phys. Rev. B 17 (1978) 1302–1322, https://doi.org/10.1103/PhysRevB.17.1302.
[19] B. Duenweg, W. Paul, Brownian dynamics simulations without Gaussian random numbers, Int. J. Mod. Phys. C 2 (1991) 817–827, https://doi.org/10.1142/s0129183191001037.
[20] S.G. Volz, G. Chen, Molecular-dynamics simulation of thermal conductivity of silicon crystals, Phys. Rev. B 61 (2000) 2651–2656, https://doi.org/10.1103/PhysRevB.61.2651.
[21] A. Bagri, et al., Thermal transport across twin grain boundaries in polycrystalline graphene from nonequilibrium molecular dynamics simulations, Nano Lett. 11 (2011) 3917–3921, https://doi.org/10.1021/nl202118d.
[22] X.-M. Yang, et al., Effects of nanobuds and heat welded nanobuds chains on mechanical behavior of carbon nanotubes, Comput. Mater. Sci. 109 (2015) 49–55, https://doi.org/10.1016/j.commatsci.2015.07.005.
[23] X.-L. Zhang, M. Hu, D. Poulikakos, A low-frequency wave motion mechanism enables efficient energy transport in carbon nanotubes at high heat fluxes, Nano Lett. 12 (2012) 3410–3416, https://doi.org/10.1021/nl300261r.
[24] W.-J. Yao, B.-Y. Cao, Triggering wave-domain heat conduction in graphene, Phys. Lett. A 380 (2016) 2105–2110, https://doi.org/10.1016/j.physleta.2016.04.024.
[25] K. Zheng, et al., An anomalous wave-like kinetic energy transport in graphene nanoribbons at high heat flux, Physica B 434 (2014) 64–68, https://doi.org/10.1016/j.physb.2013.10.050.
[26] B. Liu, et al., Interface thermal conductance and rectification in hybrid graphene/silicene monolayer, Carbon 79 (2014) 236–244, https://doi.org/10.1016/j.carbon.2014.07.064.
[27] S. Plimpton, Fast parallel algorithms for short-range molecular-dynamics, J. Comput. Phys. 117 (1995) 1–19, https://doi.org/10.1006/jcph.1995.1039.
[28] J. Tersoff, Modeling solid-state chemistry – interatomic potentials for multicomponent systems, Phys. Rev. B 39 (1989) 5566–5568, https://doi.org/10.1103/PhysRevB.39.5566.
[29] L. Lindsay, D.A. Broido, Optimized Tersoff and Brenner empirical potential parameters for lattice dynamics and phonon thermal transport in carbon nanotubes and graphene, Phys. Rev. B 81 (2010), https://doi.org/10.1103/PhysRevB.81.205441.
[30] X.-F. Xu, et al., Length-dependent thermal conductivity in suspended single-layer graphene, Nat. Commun. 5 (2014) 6, https://doi.org/10.1038/ncomms4689.